RESEARCH ARTICLE | MAY 08 2025

Nanoscale surface effects on heterogeneous vapor bubble nucleation

P. Sullivan ; D. Dockar ; R. Pillai

J. Chem. Phys. 162, 184501 (2025)
https://doi.org/10.1063/5.0259208

The Journal of Chemical Physics ARTICLE pubs.aip.org/aip/jcp

Nanoscale surface effects on heterogeneous vapor bubble nucleation

Cite as: J. Chem. Phys. 162, 184501 (2025); doi: 10.1063/5.0259208
Submitted: 18 January 2025 • Accepted: 21 April 2025 •
Published Online: 8 May 2025

P. Sullivan,[1,a)] D. Dockar,[2] and R. Pillai[2,b)]

AFFILIATIONS

[1] Department of Earth Sciences, Durham University, Science Labs, Durham DH1 3LE, United Kingdom
[2] Institute for Multiscale Thermofluids, University of Edinburgh, Edinburgh EH9 3FB, United Kingdom

[a)] **Author to whom correspondence should be addressed:** Patrick.J.Sullivan@durham.ac.uk
[b)] **Electronic mail:** R.Pillai@ed.ac.uk

ABSTRACT

Understanding the mechanisms underlying vapor bubble nucleation on solid surfaces is critical for multiple scientific and engineering applications, such as two-phase thermal management systems and turbomachinery, among others. While classical nucleation theory (CNT) explains how surface wettability influences nucleation by modifying the free energy barrier for smooth surfaces, the interplay between nanoscale surface roughness and wettability for rough surfaces remains less clear. Using molecular dynamics simulations, this study demonstrates that CNT can accurately describe wettability effects on nucleation. In addition, we show how surface cavities can create active nucleation sites without requiring trapped gases. This occurs through spontaneous dewetting of cavities at elevated temperatures, which reduces the nucleation barrier. Our results reveal that cavity-induced nucleation enhancement depends on both wettability and geometry, with dewetting promoting nucleation on lyophobic surfaces and rewetting neutralizing this effect for more lyophilic surfaces. These findings provide insights for designing surfaces to either enhance or suppress bubble nucleation.

I. INTRODUCTION

Understanding the physics governing the nucleation of vapor bubbles has been the focus of much applied research due to the numerous industrial applications. In homogeneous nucleation, spherical bubbles form in the bulk liquid region; however, bubbles are more likely to form on solid surfaces (heterogeneous nucleation), as the fluid–solid interface reduces the nucleation energy barrier.[1,2] Where bubble formation is desired, such as in two-phase thermal management systems, efforts have been made to understand how surface wettability and roughness can optimize the onset of nucleate boiling.[3–6] In contrast, where heterogeneous bubble formation is undesirable, such as in turbomachinery or on the walls of bubble chambers, masking of the solid walls has been shown to suppress bubble nucleation.[7–9] While effects of surface modifications on nucleation have been well-studied, in particular the effects of surface roughness and wettability,[10–16] there remain outstanding questions on how the coupling of these effects affects cavity wetting and, subsequently, bubble nucleation and growth.

Experimental investigations have shown that in the absence of significant surface roughness, nucleation occurs more readily on lyophobic (non-wetting) surfaces.[14] This is in agreement with the predictions of classical nucleation theory (CNT), which predicts a reduced energy barrier to nucleation when the liquid–solid interaction strength is lower.[2] In practice, many surfaces are not as ideally smooth as those assumed by CNT. Cavities on the surface further reduce the barrier to nucleation by trapping pockets of gas, forming so-called "active sites" on the surface.[1] When additional nanoscale cavities are added to the surface, the temperature at which nucleation commences has been shown to greatly decrease.[3] Conversely, when these active sites have been suppressed, by either locally cooling the walls or shielding the surface using an immiscible secondary fluid, fluids have been shown to remain in the liquid phase without nucleating, evaporating only from their free surface.[9]

Due to their importance in promoting nucleation, there have been many theoretical attempts to describe the ability of surface cavities to trap gases. Simple geometric models from Bankoff[17] and Lorenz, Mikic, and Rohsenow[18] analyzed a simple conical cavity,

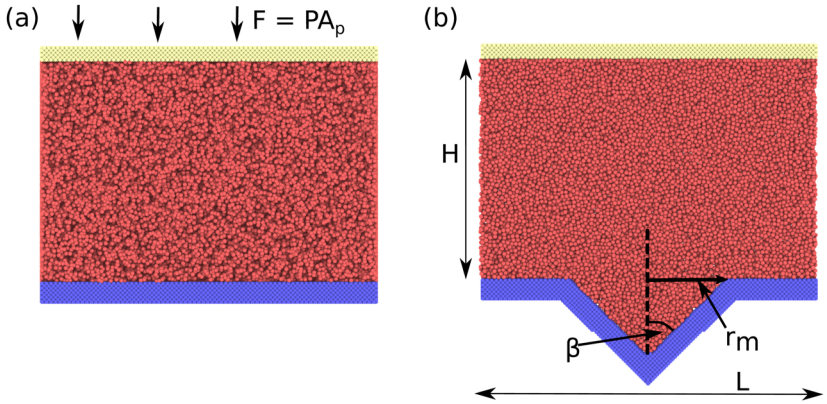

FIG. 1. Simulation setup for heterogeneous nucleation investigations. (a) System setup used for smooth surface investigations. Pressure P is controlled by applying a constant force F over the wetted area A_p of the piston molecules (yellow). (b) System used for cavity surface investigations, highlighting roughness cone angle β, cavity mouth radius r_m, height H, and length L.

defined by a mouth radius r_m and cone angle β [see Fig. 1(b)]. They predicted that a cavity would trap gas and form an active site when the contact angle of the liquid θ_l exceeded twice the cone angle i.e., $\theta_l > 2\beta$. This model was later modified by Tong *et al.*,[19] who included the effect of contact angle hysteresis, arguing that the advancing contact angle was of most importance when determining the cavity wetting state. Following a mechanical equilibrium analysis, Winterton[20] argued that gases could not be trapped when the contact angle $\theta_l < 90^\circ$. This result was corroborated by Wang and Dhir,[21] who performed a free energy minimization of a droplet sitting on top of a cavity, showing that conical cavities could not trap gas for liquids with wetting angles of less than 90°.

While these theories provide simple, geometric relationships describing the wetting state of cavities, they have proven difficult to test experimentally,[22] due to the complexities in accurately constructing a fluid–solid pairing that represents the exact conditions being modeled. An alternative technique for modeling vapor bubble nucleation is Molecular Dynamics (MD) simulation, which has become a popular tool due to its ability to natively capture phase change processes. While there has been extensive research into the nucleation of vapor bubbles on smooth surfaces[23] and on surfaces with cavities,[10,24] there remain open questions on the suitability of MD to analyze nucleation.[25] These include whether MD produces accurate descriptions of realistic fluids,[26] whether the rough surfaces used in MD are representative of realistic surfaces,[27] and whether the thermodynamic state of the system is being accurately controlled in existing nucleation simulations.[28] However, no comparisons have been made between CNT predictions and MD simulations on the effect of surface wettability on nucleation.[28] Most investigations on the role of surface wettability on bubble nucleation focus on the trade-off between the increased barrier to nucleation and the reduced interfacial thermal resistance as surfaces become more wetting.[29] While MD has been shown to well describe homogeneous nucleation rates predicted by CNT,[30,31] its ability to accurately predict heterogeneous nucleation and subsequently the effect of surface cavities on nucleation remain unclear.

In this paper, we demonstrate that MD is indeed able to match the predictions of CNT for heterogeneous nucleation. We show for the first time that, in the absence of the interfacial thermal resistances that typically dominate when liquids are heated from the contacting surface, MD simulations show excellent agreement with the nucleation temperatures predicted by CNT across the full range of surface wettabilities. Having demonstrated the suitability of MD for quantitatively capturing heterogeneous nucleation phenomena, we also investigate the effects of nanoscale surface cavities on nucleation. In order to compare against the predictions of Lorenz, Mikic, and Rohsenow,[18] we test the wetting and nucleation behavior of nanoscale conical cavities on the surface, using a range of cavity geometries and liquid contact angles. Our simulations show a complex relationship between the cavity wetting state and the combination of surface wettability and cavity cone angle, not described by existing mechanical approaches[17,18,20,21] and better resembling multi-step nucleation processes.[32]

II. SIMULATION METHODOLOGY

A. Molecular dynamics

The molecular dynamics (MD) simulations in this work were performed using the open source software LAMMPS.[33] The interactions between the atoms were calculated using the Lennard-Jones (LJ) potential,

$$U(r_{ij}) = 4\varepsilon_{ij}\left[\left(\frac{\sigma_{ij}}{r_{ij}}\right)^{12} - \left(\frac{\sigma_{ij}}{r_{ij}}\right)^{6}\right], \tag{1}$$

where σ is the characteristic length scale, ε is the potential well depth, and r is the distance between two molecules denoted by the subscripts i and j. The fluid (subscript f) interaction parameters used are $\sigma_f = 0.34$ nm and $\varepsilon_f = 0.2392$ kcal/mol, chosen to model argon.[34] The solid (subscript s) interaction parameters are $\sigma_s = 0.247$ nm and $\varepsilon_s = 15.9743$ kcal/mol, chosen to model platinum.[35] The LJ potential is truncated for values of $r > r_{cut}$, where $r_{cut} = 1.3$ nm, and simulations are performed with a time step of 5 fs using the velocity Verlet algorithm.

To investigate the effect of surface wettability, we adjust the atomic potential using the model of Nagayama and Cheng.[36] This model is based on the Lorentz–Berthelot mixing rules, which predict the effective length and energy scales for the solid–fluid interaction (subscript sf),[35] σ_{sf} and ε_{sf}, respectively, in terms of the solid and fluid values to be

$$\sigma_{sf} = b^{1/6}\frac{\sigma_s + \sigma_f}{2}, \tag{2}$$

TABLE I. LJ scaling factors for varying wettability surfaces with approximate droplet contact angles.

b	θ_l [°]
0.9	10
0.7	40
0.65	55
0.6	70
0.5	95
0.45	105
0.4	120
0.3	150

$$\varepsilon_{sf} = ab^2\sqrt{\varepsilon_s\varepsilon_f}. \tag{3}$$

Their model[36] incorporates the modifications made by Din and Michaelides[37] to the magnitude of the potential as well as by Barrat and Bocquet[38] to the attractive portion of the potential. There are two scaling factors; the factor a scales the magnitude of the potential, while the factor b adjusts the balance of attractive to repulsive components.

To achieve a range of partial wetting cases, a fixed value of $a = 0.14$ was used,[39] allowing for wettability to be controlled by b alone.[38] The values of b used, and the corresponding contact angles, are given in Table I.[40]

B. Simulation setup

Three types of simulation setups are used in this work, for the study of (a) homogeneous nucleation, (b) heterogeneous nucleation on a smooth surface, and (c) heterogeneous nucleation on a cavity-containing surface. These setups have some minor differences, which are discussed later in this section. The simulation methodology employed in all cases involves slowly raising the temperature of an isobaric fluid until nucleation occurs. Initially, the system is equilibrated to a constant pressure of $P = 0.1$ MPa and a temperature of $T_0 = 100$ K. While these conditions would provide a supersaturated state for liquid argon, the supersaturation is not sufficient for nucleation to occur in the time and length scales practically achievable with MD.[41] The temperature of the system is then raised to increase the supersaturation, which is achieved using a two step process. First, the system temperature is ramped up from its starting temperature T_0 to a higher temperature $T_0 + \delta T$. This is done over a time-frame of 0.5 ns to minimize transient effects from rapidly heating the fluid. The fluid is then allowed to equilibrate again at this higher temperature for a further 0.5 ns. These timescales were chosen to allow for sufficient time to elapse during the simulations for nucleation to occur and be detected while still being computationally feasible. This process is then repeated until nucleation occurs. δT was set to 2 K to find an approximate nucleation temperature, before a second set of simulations with a smaller value of $\delta T = 0.5$ K was conducted to more precisely calculate the nucleation temperature. To ensure that our heating rate was suitable for comparing against CNT, we found no dependence with the heating rate on nucleation temperature up to 8 K/s (see the supplementary material). The presence of a nucleated bubble is determined by a sharp and sustained drop in molecule number density in the simulation domain,[30] reaching an average molecule number density below 10 molecules/nm^3.

1. Homogeneous nucleation

To measure homogeneous nucleation rates, the simulations are performed using a cubic simulation domain of length 10 nm under periodic boundary conditions, consisting of just fluid molecules. This simulation is performed in the NPT ensemble, where the temperature and pressure of the homogeneous fluid are controlled using Nosé–Hoover thermostats and barostats, respectively.

2. Heterogeneous nucleation

The investigations into heterogeneous nucleation are performed initially on cavity-free, atomically smooth surfaces [see Fig. 1(a)]. Subsequent simulations are performed on surfaces with simple conical cavities [see Fig. 1(b)]. For both sets of simulations, the fluid is contained between two fixed FCC surfaces. The lower surface (blue atoms in Fig. 1) has its wettability modified as described above and is the surface on which nucleation will occur in these simulations. It is also the surface on which the cavities will be inserted for the cavity surface simulations. The upper surface (yellow atoms in Fig. 1) is used as a piston to control the system pressure by applying a fixed force to each of the piston atoms; the implementation of the piston is described in our previous study.[40,42,43] The use of the piston allows for accurate control of the system pressure, which is needed to compare simulation results against CNT[44] and is missing from previous investigations.[28] The system setup used for the smooth surface MD simulations is shown in Fig. 1(a). The critical radius for nucleation at a temperature of 134 K is of order 3 nm, which is ten times smaller than the simulation domain used for the smooth surface investigations of 30 nm, with an investigation into the effect of the domain size presented in the supplementary material.

The role of roughness is investigated here by using simple conic cavities on the solid surface defined by a combination of the cone angle β and the cavity mouth radius r_m. The cone is then filled with liquid, as illustrated in Fig. 1(b). The system height H is set to be at least three times the cavity mouth radius r_m and length L at least four times the cavity radius. Controlling the cavity radius and cone angle allows for the comparison to the predictions of the site activation criteria of Lorenz, Mikic, and Rohsenow[18] and Winterton.[20]

III. RESULTS AND DISCUSSION

The results of these simulations are compared to the predictions of CNT. A detailed description of the theory is provided in the Appendix, with derivations of all the necessary equations used here. The most relevant parameters to this investigation are the critical radius R_c and the nucleation rate J. The critical radius is the radius of curvature above which it is energetically favorable for the nucleus to grow and below which the bubble will instead collapse. For spherical and cap shaped bubbles, the critical radius is given as

$$R_c = \frac{2\gamma}{\Delta P}, \tag{4}$$

where γ is the liquid–vapor surface tension and ΔP is the difference between the internal bubble pressure (including curvature effects from the Kelvin equation) and external liquid pressure.

The nucleation rate, or the expected number of nucleation events to occur per unit time in a given volume, is expressed as

$$J = J_0 e^{-\Delta G_c / k_B T}. \tag{5}$$

Here, J_0 represents the kinetic limiting nucleation rate, the maximum rate that nucleation would occur at if there were no energy barrier. The energy barrier term ΔG_c represents the free energy needed to create a critically sized nucleus; k_B is the Boltzmann constant, and T is the temperature.

Having computed the nucleation rate from Eq. (5), the probability of a bubble forming in a given volume V (in the case of homogeneous nucleation) over a specified time period t can be calculated, assuming a Poisson distribution of nuclei sizes,[45] as

$$p_{nuc} = 1 - e^{-JVt}. \tag{6}$$

In the case of heterogeneous nucleation, the volume term is replaced by the surface area A over which nucleation can occur,

$$p_{nuc} = 1 - e^{-JAt}. \tag{7}$$

The use of a Poisson distribution to describe the nucleation of condensed phases has been widely employed.[46] The same governing principles are applicable to the formation of gaseous phases,[1] with Gallo and Casciola[47] demonstrating that the distribution of heterogeneous bubble nucleation sites is well described as a random Poisson process.

A. Effect of surface wettability

In order to investigate the role of surface wettability on the nucleation of vapor nanobubbles, we perform MD simulations to determine the nucleation temperature of a homogeneous vapor bubble as a benchmark. The homogeneous nucleation temperature for argon at 0.1 MPa was measured to be 134 ± 0.5 K, using our method described earlier. The theoretical model based on CNT in Eq. (6) predicts that a vapor bubble will have nucleated by this temperature with a probability of greater than 50%, which is the threshold we will use in the remainder of this investigation. This agreement between MD predictions and 50% probability threshold for CNT highlights the suitability of CNT to describe vapor bubble nucleation. As nucleation is a stochastic process, we perform six realizations of the nucleation simulations in order to statistically describe the system. This stochasticity is highlighted by the formation of bubbles in different locations on the surface in different simulation realizations, with images of bubbles forming in different locations in different simulations presented in the supplementary material.

Figure 2 shows the measured nucleation temperatures of vapor bubbles on surfaces of various wettabilities from MD simulation compared to the predictions from CNT. The CNT temperatures are taken as the value at which Eq. (7) predicts a nucleation probability of 50%. There is good agreement between the CNT predictions and measured temperatures across the whole range of wettabilities, with all of the observed temperatures sufficiently below the 141 K spinodal temperature of LJ argon at a system pressure of 0.1 MPa.[48]

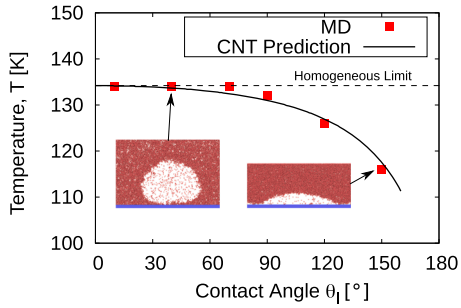

FIG. 2. Temperature at which bubble nucleation occurs on smooth surfaces of varying wettabilities for liquid argon at a pressure of 0.1 MPa. The dashed line represents the temperature at which homogeneous nucleation occurs. The insets show representative simulation snapshot segments of bubbles on surfaces with $\theta_l = 40°$ and $\theta_l = 150°$.

The nucleation temperature is reduced on the lyophobic surfaces (i.e., for $\theta_l > 90°$) because of the corresponding reduction in the barrier to nucleation. Interestingly, the nucleation temperature reaches a constant value of 134 K for lyophilic surfaces (i.e., for $\theta_l \leq 90°$), matching the value for the homogeneous case. The apparent independence of the nucleation temperature from the contact angle on highly wetting surfaces is a similar behavior to that observed by Gallo *et al.*,[49] who performed stochastic mesoscale simulations of boiling, although is in disagreement with several existing MD studies on vapor bubble nucleation, which report preferential nucleation on lyophilic surfaces.[10,35] These studies heat the fluid by thermostatting the solid surface. Surface heating introduces an additional solid/liquid interfacial thermal resistance, which can be dominant at the molecular scale and is greater for lyophobic surfaces.[28,29] When, instead, we heat the liquid directly and remove interfacial heat transfer effects using an adiabatic surface, we recover the predictions of CNT and observe that bubbles nucleate preferentially on lyophobic surfaces.

B. Effect of surface topography

The temperatures at which nucleation occurs on surfaces with $r_m = 10$ nm cavities for various cone angles and wettabilities are shown in Fig. 3. For comparison, the smooth surface case is also included and can be thought of as corresponding to a surface with a cone angle of $\beta = 90°$. It is important to note that for this investigation, we measure the temperature at which we see sustained bubble growth out of the surface cavity, rather than the temperature at which the cavity dewets (which, in itself, can be regarded as a nucleation event[50]).

In Fig. 3, we see that for the highly wetting surfaces, there is no effect of the cavity shape on the nucleation temperature, with all lines lying on top of one another for the $\theta_l \leq 70°$ surfaces. However, as the wettability is decreased (i.e., θ_l is increased), the temperature at which a bubble nucleates and continues to grow on the cavity surfaces is reduced for the less wetting surfaces (i.e., when $\theta_l \gtrapprox 90°$). This is due to the dewetting of the cavity as the system heats, where the cavity acts as a pre-existing active site with a reduced energy barrier associated with the continued growth of the bubble out of the cavity.[2] All the cavity surfaces lie below the corresponding smooth

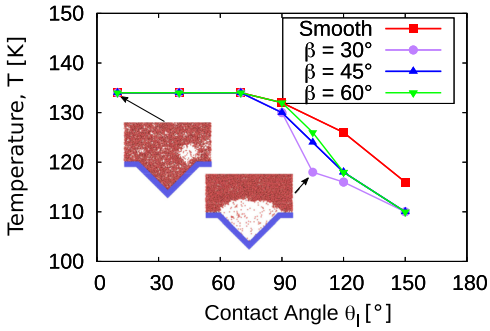

FIG. 3. Temperature at which a stable bubble continuously grows from a r_m = 10 nm radius cavity for various wettabilities and cone angles β compared to a cavity-free surface. The insets show simulation snapshots of bubble nucleation in $\beta = 45°$ cavities for $\theta_l = 10°$ and $\theta_l = 105°$.

surface values (red line) in Fig. 3. Notably from these results, we see that the temperature at which the cavity dewets, and subsequently the temperature at which we see stable bubble growth, is significantly lower for the $\beta = 30°$ cone angle on the $\theta_l = 105°$ wettability surface, increasing as the cone angle increases. In addition, the nucleation temperature is slightly lower for smaller cone angles on the $\theta_l = 90°$ and $\theta_l = 120°$ surfaces, with the $\beta = 30°$ cases (purple circles) showing the lowest nucleation temperatures. This reduced temperature for nucleation in lower cone angle cavities vanishes for the least wetting surface ($\theta_l = 150°$), where the continuous bubble growth occurs at the same temperature regardless of cone angle, i.e., the three curves show bubble growth at the same temperature. The nucleation temperature on the cavity surfaces for $\theta_l = 150°$, despite being the same regardless of cone angle, is still lower than the nucleation temperature on the smooth surface with the same wettability.

Next, we focus on the role of cavity geometry and surface wettability on wetting behavior. The images in Fig. 4 show two surfaces with the same cavity geometries, but different wettabilities, demonstrating different cavity wetting behaviors. On the more wetting surface ($\theta_l = 10°$) in Fig. 4(a), the cavity remains wetted throughout the simulation procedure. In the case of the less wetting surface ($\theta_l = 150°$) in Fig. 4(b), the cavity dewets during the equilibration procedure, forming a vapor-filled cavity. The liquid–vapor interface above the cavity appears flat in this case. This can be explained by

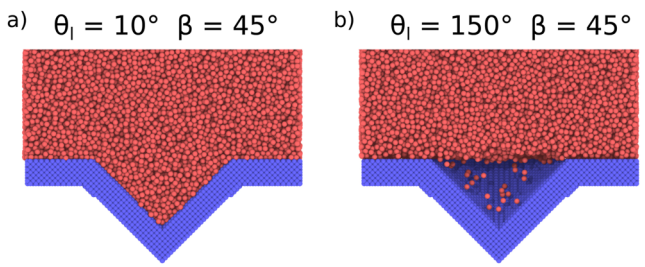

FIG. 4. Comparison of the wetting state for identical cavities on surfaces with two different wettabilities. The cavity remains wetted on the (a) $\theta_l = 10°$ surface but dewets on the (b) $\theta_l = 150°$ surface.

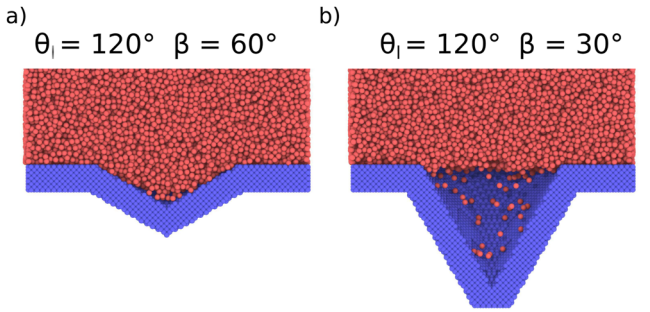

FIG. 5. Comparison of the wetting state for identical cavities on surfaces with two different wettabilities. The cavity remains wetted on the cavity with (a) $\beta = 60°$ but dewets on the cavity with (b) $\beta = 30°$.

the results of Xiao *et al.*,[51] who showed that the radius of curvature of a pinned surface vapor nanobubble matches the critical radius at the particular thermodynamic state (i.e., temperature and pressure) of the system. By matching the critical radius, the pinned bubble can exist in a mechanical equilibrium with the surrounding liquid. In the case of Fig. 4(b), as the critical radius from Eq. (4) is significantly larger than the cavity radius ($R_c \approx 85$ nm $\gg r_m$), the interface appears flat. This configuration is more energetically stable as creating a curved interface would increase the interfacial free energy enough to more than offset the reduction obtained by allowing more molecules to vaporize. As the temperature increases and the critical radius becomes smaller, the interface curves to reach a mechanical equilibrium, as described by Eq. (4).

Similarly, Fig. 5 shows two surfaces with the same wettability and different geometry cavities. The cavity remains completely wetted for the setup with a cone angle $\beta = 60°$ [Fig. 5(a)]. When the cone angle is reduced to $\beta = 30°$ [Fig. 5(b)], the wetting behavior changes, and the cavity spontaneously dewets during equilibration. Again, when the cavity has dewetted, a flat liquid–vapor interface forms, rather than the convex interface that would match the liquid contact angle, as it is assumed in the analysis of Lorenz, Mikic, and Rohsenow.[18] This shows the importance of the interplay between the cavity shape and fluid–surface interaction strength on the resulting wetting state.

We can identify two distinct wetting regimes throughout these simulations. The cavities either (a) remain wetted during the equilibration process or (b) dewet and fill with vapor. These approximately correspond to the Wenzel and Cassie–Baxter wetting states at the macroscale, respectively.[52,53] We have seen that the preferred state of the system, whether the cavity is wetted or dewetted, is controlled predominantly by the wettability of the surface and the geometry of the cavity. Higher wettability surfaces (i.e., lower θ_l) and less steep cavities (i.e., higher β) are more likely to remain wetted. Having identified the two wetting regimes, their effect on vapor bubble nucleation can now be investigated. From the MD simulation results, a clear difference between the two regimes is observed:

1. Wetted cavities

The simulation results in the wetted cavity regime do not differ significantly from the results of the smooth surface investigations;

this can be seen in Fig. 3, where the nucleation temperature for the lyophilic surfaces when $\theta_l \leq 90^\circ$ is independent of the presence of the cavity. The temperature required for nucleation to occur is identical in both cases. This shows that a completely wetted cavity does not significantly reduce the barrier to nucleation in the cases tested.

2. Dewetted cavities

A distinctly different nucleation behavior is observed for dewetted cavities. When the cavity has dewetted, the vapor trapped in the cavity acts as a pre-existing nucleus and, therefore, a site at which nucleation can preferentially occur.[1] The presence of these sites reduces the barrier to nucleation, potentially allowing bubble growth to occur at lower superheats.[54] These dewetted cavities produce bubbles pinned to the cavity mouth with a base radius equal to the cavity radius r_m. It has been shown that pinned vapor bubbles have a radius of curvature matching the critical radius, as predicted by nucleation theory at the temperature and pressure at which they exist.[51] The radius of curvature of these bubbles can be given in terms of the cavity mouth radius and the apparent liquid contact angle relative to the flat solid surface θ_a as

$$R = \frac{r_m}{\sin\theta_a}. \tag{8}$$

In the case of the flat liquid–vapor interfaces shown in Figs. 4(b) and 5(b), the apparent contact angle is taken as completely non-wetting, i.e., $\theta_a = 180^\circ$, and drops as the bubble volume increases. The bubble will remain pinned and not grow out of the cavity until this apparent angle θ_a reaches the intrinsic liquid contact angle of the surface θ_l, at which point it grows with a constant contact angle.

Figure 6 shows the measured nucleation temperatures on dewetted cavity surfaces with different mouth radii for several different wettabilities. These mouth radii are converted into bubble radii of curvature using Eq. (8). Good agreement is seen between the simulation results and theoretical predictions for $\theta_l = 90^\circ$ with a slight overprediction for $\theta_l = 120^\circ$. Notably, for the least wetting surface ($\theta_l = 150^\circ$), the simulation results do not match the predictions of CNT given by the solid black line for small radii. For this surface, the critical nucleation temperature is 116 K (in the absence of a cavity), as shown in Fig. 2, which is less than the temperature required to produce the critical radius given by Eq. (8) (124 K) for a 6 nm radius nanobubble. As a result, nucleation occurs at the lower temperature for a cavity-free surface, i.e., the surface cavity does not enhance nucleation. When the cavities become sufficiently large, the nucleation temperature reduces, matching the predictions of CNT in the solid black line. This indicates that for highly lyophobic surfaces, a threshold cavity radius exists only above which significant nucleation enhancement occurs.[50] This cavity radius is equivalent to the base radius of a nucleating bubble on a smooth surface.

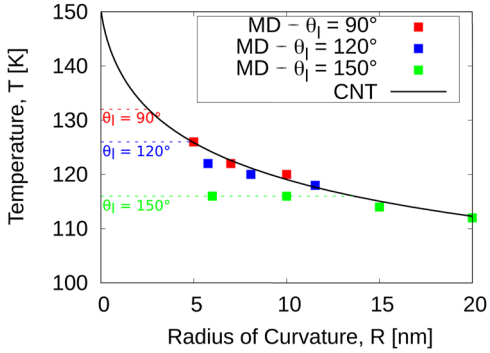

FIG. 6. Comparison of the nucleation temperature on different wettability surfaces to the predictions of nucleation theory for cavities of various radii. The radius value on the x axis represents the radius of curvature of a bubble with a base radius equal to the cavity radius. The dashed lines represent the temperature at which nucleation occurs on a smooth surface for each wettability.

C. Identifying wetting regimes

Having shown the importance of the wetting state to the nucleation behavior of surfaces, an important open question remains: *what decides the wetting state of a given surface?* The analysis of Lorenz, Mikic, and Rohsenow[18] would suggest that it depends on exclusively the cone angle β and liquid contact angle θ_l and that the wetting state is determined during the filling of the cavity with fluid. This analysis would suggest that cavities would exist in the dewetted state when

$$2\beta < \theta_l, \tag{9}$$

and in the wetted state when

$$2\beta \geq \theta_l. \tag{10}$$

A free energy analysis of cavity wetting states by Giacomello *et al.*[50] describes the cavity wetting state as additionally depending on the ratio of the cavity radius to the critical radius of the bubble at the specific temperature and pressure. This analysis shows that cavities cannot remain in the wetted state when

$$\beta < \theta_l - 90^\circ. \tag{11}$$

When the inequality in Eq. (11) does not hold, the cavity can still exist in the dewetted state, provided that

$$\beta < \theta_l - \left(90^\circ - \sin^{-1}\left(\frac{r_m}{R_c}\right)\right). \tag{12}$$

This expression highlights the dependence of the wetting state on the thermodynamic state of the system through the ratio of the cavity radius to critical radius. It is worth noting that in the limit of low supersaturation (i.e., high R_c) or large cavity radii Eq. (12) simplifies to Eq. (11).

In order to test these criteria, we perform two sets of tests: cavities initially filled with liquid and cavities initially filled with vapor. We investigate whether the cavities remain filled with liquid or dewet and whether the cavities remain dewetted or refill with liquid across a range of wettabilities and cone angles. We perform these simulations on surfaces with cavities with a mouth radius $r_m = 5$ nm and at a temperature of 100 K, as before. Simulations are run for up to 5 ns to ensure complete rewetting or dewetting of the cavities. The resulting wetting states are shown in Fig. 7, with the dashed black lines representing the cavity wetting criteria from Eqs. (9) and (11).

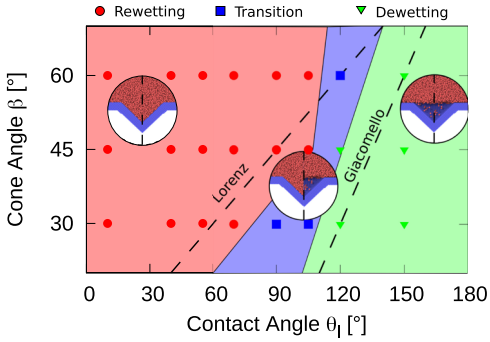

FIG. 7. Regime map indicating the wetting states for cavities of varying cone angles β and surface wettabilities θ_l. Cavities that rewet when equilibrated dewetted are shown with the red circles. Cavities that dewet when equilibrated wetted are shown with the green triangles. Cavities that do not change from their initial wetted state are shown by the blue squares. The cavity wetting criteria predicted by Lorenz, Mikic, and Rohsenow[18] and Giacomello *et al.*[50] are represented by the dashed black lines. The insets are representative snapshots of simulations highlighting the wetting state for the initially filled (left) and unfilled (right) cavities.

It is worth emphasizing at this point that the exact wetting state of the cavity will be dependent on both the system temperature and the simulation time, as the transition from the wetted to dewetted cavity is itself an activated nucleation phenomenon.[32]

We can see from these results that three distinct regimes emerge. For the lyophobic surfaces ($\theta_l > 120^\circ$) with smaller cone angles, the cavities are always dewetted for the cone angles tested, as predicted by Lorenz's theory [Eq. (9)]. For lyophilic surfaces with $\theta_l < 70^\circ$, the cavity is always filled, regardless of the cone angle or initial wetting state, as per Eq. (10). Lorenz's theory fails to predict the rewetting of some of the cavities, specifically when $\theta_l = 70^\circ$ and $\beta = 30^\circ$ and $\theta_l = 105^\circ$ and $\beta = 45^\circ$. The $\theta_l = 120^\circ$ and $\theta_l = 105^\circ$ surfaces with a cavity angle of $\beta = 30^\circ$ and $\theta_l = 120^\circ$ and $\beta = 30^\circ$ surfaces show a clear dependence on the initial wetting state of the cavity. If the cavity begins wetted, it remains wetted throughout the simulation; however, when the cavity is initialized in a dewetted state, it will not rewet. This result shows that the geometric gas trapping model of Lorenz, Mikic, and Rohsenow[18] does not accurately capture the cavity wetting state at the nanoscale. The hysteresis observed in the wetting state of the cavities cannot be captured by this type of mechanical macroscale theory. We see a better agreement with the predictions of Giacomello *et al.*,[50] with Eq. (11) identifying when the cavity is consistently dewetted. Some of the hysteresis seen in the transition region can be attributed to the energetically activated, nucleation style dewetting that can occur when the inequality in Eq. (12) is satisfied; however, this does not quantitatively explain all of the results seen here. For a cavity radius of 5 nm and a critical radius of 85 nm, a value of $\sin^{-1}\left(\frac{r_m}{R_c}\right) \approx 3.5^\circ$ is obtained, which is not sufficient to explain the exact location of the wetting–dewetting transition.

Using the understanding of the wetting behavior of surface cavities shown in Fig. 7 and the variation in nucleation temperatures shown in Fig. 6, we can better interpret the results of nucleation temperatures seen in Fig. 3. For the highly wetting surfaces ($\theta_l < 70^\circ$), the cavities remain filled and nucleation occurs in a single step, equivalent to nucleation on a smooth surface. As the wettability is decreased, bubble nucleation occurs within the cavity, with nucleation occurring preferentially for smaller cone angles. In the cases when this cavity nucleation occurs at a temperature above that at which a stable bubble can grow from the cavity, which is defined by the cavity mouth radius and wetting angle, the formation and growth of a bubble is again a single step process. This explains the reduction in the reported temperature for the $\beta = 45^\circ$ and $\beta = 60^\circ$ on the $\theta_l = 105^\circ$ surface in Fig. 2, where continuous bubble growth occurs immediately as the cavity dewets.

When the cavity mouth radius exceeds the critical bubble base radius at the dewetting temperature, nucleation becomes a two-step process.[32] The first step involves the transition from the wetted to dewetted cavity state and the second from the dewetted cavity state to a bubble continuously growing outside the cavity. The thermodynamics of this two-step nucleation has been extensively analyzed by Giacomello *et al.*,[50] who have similarly identified single and multi-step nucleation regimes governed by the combination of cavity geometry and surface wettability. The regimes identified in their work align well with the conditions observed in our molecular simulation, notably with Eq. (8) describing the growth of bubbles from dewetted cavities and the transition from one to two-step nucleation as wettability is changed.

These simulation results illustrate the complex interactions between surface geometry and wettability, which produce lower barriers to the nucleation of vapor bubbles. While CNT has been shown to accurately predict nucleation on atomically smooth surfaces, the presence of surface cavities has been shown to alter this behavior (see Fig. 3). The transition between wetting and non-wetting cavity states, as well as the observed hysteresis in this transition, is therefore crucial to predicting when continuous bubble growth will be observed. The role of nanoscale interfacial phenomena, such as the line tension along the three phase contact line,[55] surface adsorption,[40,56] and non-continuum energy landscape in the cavity,[35] therefore, warrants further investigation to understand temperature driven transition in the wetting behavior of these cavities and enables the development of more accurate theoretical models.[57] This could include an extension of the thermodynamic modeling in Giacomello *et al.*[50] and of the probabilistic modeling presented in this work to account for the altered nucleation kinetics that occur inside nanoscale surface cavities.

IV. CONCLUSIONS

In this work, we have investigated how the formation of vapor bubbles is affected by the presence of a solid surface. Using molecular dynamics (MD) simulation, we explored the temperature at which a vapor bubble forms on surfaces ranging from highly wetting ($\theta_l = 10^\circ$) to highly non-wetting ($\theta_l = 150^\circ$). By including conical cavities of various mouth radii r_m and cone angles β, we explore how surface roughness can alter the bubble nucleation temperature.

We first compare the temperature at which nucleation occurs on atomically smooth surfaces in our simulations to those predicted by classical nucleation theory (CNT). This is achieved in our simulations by heating the fluid uniformly, rather than heating the fluid using the solid surface, as is common in other investigations.[35,58] By removing the effects of interfacial thermal resistance, which has been shown to dominate in previous investigations into the effect of

wettability on nucleation,[28] we show that CNT accurately predicts the nucleation temperature across the entire range of wettabilities investigated.

Extending this investigation to surfaces with conical cavities, we identify the coupled effects of surface roughness and wettability on nucleation temperature. We show that for less wetting surfaces ($\theta_l > 90°$), the presence of a 10 nm radius surface cavity can reduce the nucleation temperature by over 10 K. This reduction in nucleation temperature is driven by a transition from wetted to dewetted cavities. We show that cavities are more likely to dewet for higher θ_l (lower wettability) and lower β (narrower cones). When the cavities dewet, they act as pre-existing nuclei, providing locations with a reduced energy barrier for nucleation. Bubbles are shown to continuously grow from these cavities when their radius of curvature matches the critical radius predicted from CNT. In the extreme of low wettability and small cavity radii, nucleation is shown to occur as if no cavity is present.

Comparing the observed wetting state for various combinations of wettability and cavity geometry, we reveal a dependence on the initial wetting state on the transition between the wetted and dewetted cavity regimes. This is not captured by the predictions of mechanical models for the cavity wetting state,[18,20] highlighting that this transition is an activated nucleation phenomenon. Understanding the complete picture of cavity dewetting will give further insight into the factors that affect nucleation on realistic macroscale surfaces. These insights into the influence of molecular scale surface interactions on vapor bubble nucleation will guide the design of surfaces to better control, either enhance or limit, the formation of bubbles.

SUPPLEMENTARY MATERIAL

See the supplementary material for additional information on the effects of domain size and heating rate on the nucleation temperature observed in our simulations, as well as visualizations of the formation of bubbles at different locations on smooth surfaces in different simulation realizations.

ACKNOWLEDGMENTS

We thank two anonymous reviewers for their contributions to the article. Duncan Dockar is supported by the Royal Academy of Engineering under the Research Fellowship program. Rohit Pillai is supported by the UKRI Frontier Guarantee Grant No. EP/Y036107/1. This work made use of the Hamilton HPC Service of Durham University.

AUTHOR DECLARATIONS

Conflict of Interest

The authors have no conflicts to disclose.

Author Contributions

P. Sullivan: Conceptualization (lead); Methodology (lead); Writing – original draft (lead). **D. Dockar**: Methodology (supporting); Supervision (supporting); Writing – review & editing (equal). **R. Pillai**: Supervision (lead); Writing – original draft (supporting).

DATA AVAILABILITY

The data that support the findings of this study are openly available in Durham University's Collections Repository at https://doi.org/10.15128/r1mc87pq34z.[65]

APPENDIX: NUCLEATION THEORY

Nucleation is dependent on two competing effects: a material that exists in an energetically unfavorable phase trying to change state and an energy barrier to create a new phase boundary. In order for the material to change from the old, energetically unfavorable phase to the new one, an initial seed, or nucleus, must form with enough energy to exceed the energy barrier of the new phase.[1]

The driving force for nucleation is the difference between the chemical potential of a molecule in the old and new phases, termed the supersaturation $\Delta\mu$. The supersaturation associated with the formation of a vapor bubble can be determined by taking the difference between the free energies of the fluid in the vapor and liquid states,[1] given here in terms of the saturated vapor pressure P_{sat} and the liquid pressure P_∞,

$$\Delta\mu = k_B T \ln\left(\frac{P_{sat}}{P_\infty}\right) - v_0(P_{sat} - P_\infty). \tag{A1}$$

For the analysis of bubbles, the driving force is typically given in terms of the fluid underpressure ΔP, the difference between the pressure inside the bubble P_b and the pressure in the fluid P_∞, i.e., $\Delta P = P_b - P_\infty$. Here, the pressure in the bubble is given by[2]

$$P_b = P_{sat} e^{-\frac{v_0(P_\infty - P_{sat})}{k_B T}}, \tag{A2}$$

where k_B is the Boltzmann constant, T is the temperature of the fluid, and v_0 is the molecular volume.

The barrier to the formation of a new phase arises from the additional free energy required to form the interface between the two phases. This interfacial excess energy γ arises from the force anisotropy experienced by the molecules at the interface.[52,53] In the case of a liquid interface with its own vapor, this excess energy is often referred to as *surface tension*, as it is indistinguishable from the interfacial stress.[59]

Taking the difference between the barrier resisting nucleation and the energetic driving force, the change in Gibbs free energy ΔG associated with the formation of a nucleus can be given as[1]

$$\Delta G = -n\Delta\mu + \gamma A, \tag{A3}$$

where n is the number of molecules in the nucleus and A is the interfacial area. In the case of vapor bubbles, it is often more useful to express the Gibbs free energy in terms of pressure difference.[1,2] For the case of a spherical vapor nucleus, the Gibbs free energy $\Delta G(R)$ change is expressed in terms of the radius as[1]

$$\Delta G(R) = -\frac{4}{3}\pi R^3 \Delta P + 4\gamma\pi R^2. \tag{A4}$$

This expression gives a clearer picture of the relationship between the change in Gibbs free energy and the size of the nucleus.

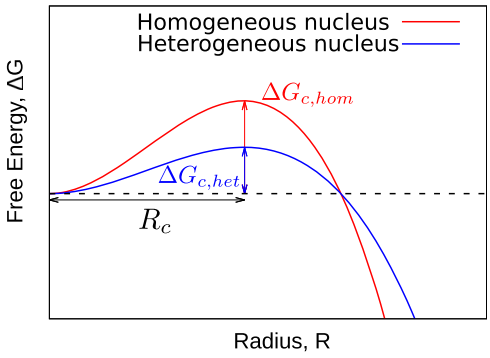

FIG. 8. Illustration of change in Gibbs free energy of a nucleus of a given radius. The maximum value of free energy ΔG_c is lower for heterogeneous nuclei, but the critical radius R_c is equal for both homogeneous and heterogeneous nuclei.

For large nuclei, the volumetric supersaturation term dominates as it scales with R^3. In these cases, it is energetically favorable for the nucleus to grow indefinitely. Meanwhile, for small nuclei, the surface area term dominates as it scales with R^2. Here, it is energetically favorable for the nucleus to shrink, reducing the interfacial surface area, despite the supersaturation.

This means there is a critical value of nucleus radius R_c above which it is energetically favorable for the nucleus to grow and below which it is favorable for it to shrink. This can be seen qualitatively in the plot in Fig. 8, which visualizes how the Gibbs free energy changes with radius. The energy barrier that must be overcome (ΔG_c) is the value of the change in free energy of a critically sized nucleus. We can obtain an expression for the critical radius by finding the location of the maximum of Eq. (A4) by setting the first derivative with respect to R as 0, i.e., $\frac{\partial \Delta G}{\partial R} = 0$,

$$R_c = \frac{2\gamma}{\Delta P}. \tag{A5}$$

Notably, this expression is identical to the Young–Laplace equation, relating the pressure change across a curved interface to its radius of curvature. This shows that in order for a nucleus to grow, the pressure difference ΔP must exceed the Laplace pressure of a bubble with radius R_c. It has been shown that the value of surface tension γ is dependent on the curvature of the interface on which it is acting.[60] The value of effective surface tension for a curved interface is typically given in terms of the planar surface tension γ_0 and a length scale δ_T, referred to as the Tolman length,[61] as

$$\gamma = \frac{\gamma_0}{\left(1 + \frac{2\delta_T}{R}\right)}, \tag{A6}$$

with R here being the radius of curvature of the interface. For this investigation, we use a value of $\delta_T = 0.34$ nm.[62]

In the case of heterogeneous nuclei, where the new phase forms at a surface, the same energy balance approach can be used. However, the volume and surface area terms must be scaled to account for the change in geometry of the nucleus. For spherical cap shaped nuclei, the free energy of the nucleus becomes a function of both the radius and contact angle θ_v (where θ_v is the vapor side contact angle) that the nucleus makes with the solid surface. In addition, the interfacial free energy between the nucleus and surface must be considered in the calculations. This results in a scaling of the free energy by a factor of

$$\psi(\theta_v) = \frac{(2 + \cos\theta_v)(1 - \cos\theta_v)^2}{4}. \tag{A7}$$

This factor ψ always takes a value between 0 and 1, indicating that heterogeneous nucleation always requires a lower energy barrier to be overcome than homogeneous nucleation at the same supersaturation. This can be seen in Fig. 8, which illustrates how ΔG_c for a homogeneous nucleus is greater than that for a heterogeneous nucleus. Accounting for the effect of the modified bubble geometry on the Gibbs free energy associated with the supersaturation and creation of the liquid–vapor and vapor–solid interfaces, Eq. (A4) can be rewritten for heterogeneous nucleation as[1]

$$\Delta G(R, \theta_v) = \frac{(2 + \cos\theta_v)(1 - \cos\theta_v)^2}{4}\left(-\frac{4}{3}\pi R^3 \Delta P + 4\gamma\pi R^2\right). \tag{A8}$$

Finding the location of the maximum of Eq. (A8) by differentiating with respect to R returns the Young–Laplace equation, indicating that the critical radius is identical for homogeneous and heterogeneous nuclei. However, the value of the free energy barrier is reduced by $\psi(\theta_v)$. In addition, Eq. (A8) shows that ΔG_c is lower for low values of θ_v. This matches experimental observations, where vapor bubbles form at lower superheats on less wetting surfaces.[2,3]

1. Nucleation kinetics

While the thermodynamics of nucleation as described above can determine the Gibbs free energy barrier to nucleation and the size of the critical nucleus, it does not tell us about the likelihood of this barrier being overcome and critical nucleus forming. This energy barrier ΔG_c measures the free energy penalty that must be overcome in order for a nucleus to exceed the critical size. The kinetics of nucleation theory investigates the rate J at which critical nuclei can be expected to form. In the case of isothermal nucleation at constant supersaturation, the nucleation rate can be expressed as[1,63]

$$J = J_0 e^{-\Delta G_c / k_B T}. \tag{A9}$$

The exponential term shows that the energy barrier ΔG_c plays a significant role in determining the nucleation rate. The prefactor J_0 determines the kinetic contribution to the nucleation rate. This is a measure of the rate at which nucleation would occur without an energy barrier and can be expressed as[1]

$$J_0 = \Gamma\sqrt{\frac{c^3\gamma}{18\pi^2 m_0}}C_0. \tag{A10}$$

This depends on the molecular mass of the particles m_0 and a particle attachment factor Γ, which is typically taken as unity.[1,30] C_0 is the density of nucleation sites, with units of m^{-3} for homogeneous nucleation and m^{-2} for heterogeneous nucleation. The effect of the

shape of the nucleus is captured in c^3, a factor that, for spherical caps, is given as

$$c^3 = \frac{36\pi}{2 + \cos\theta_v}. \tag{A11}$$

In the case of spherical nuclei, this shape factor simplifies to 36π. In the case of homogeneous nucleation, C_0 has units of sites per unit volume. For pure substances, there are no alternative nucleation sites, so the site density is equal to the particle number density.[60] The nucleation rate J will then have units of nucleation events per unit volume per unit time. For heterogeneous nucleation, the site density is given as the number of active sites per unit surface area, which, for atomically smooth surfaces, is one site per unit lattice surface area.[1] This value can vary significantly for irregular surfaces depending on the surface geometry and subsequent number of preferential nucleation sites.[2] Roughness on the solid surface often allows for pre-existing nuclei to reduce the energy barrier to nucleation, causing a significant increase in the nucleation rate and allowing nucleation to occur at lower supersaturations.[3,24]

The exact form of the equation used to describe the kinetic limit of nucleation J_0 depends on the assumptions made in determining the limiting behavior. An overview of several of the different factors affecting this is given by Blander, Hengstenberg, and Katz.[64] An investigation into several of these different equational forms by Rosales-Pelaez *et al.*[30] showed that in the case of homogeneous vapor bubble nucleation, several of the commonly used expressions agreed within an order of magnitude. Given the orders of magnitude change in nucleation rate per Kelvin change in temperature,[30] these differences in J_0 are taken as an acceptable error. This is particularly relevant when compared to the orders of magnitude difference in nucleation rate that are observed by including the effects on bubble pressure captured by Eq. (A2) and the Tolman length effect on surface tension by Eq. (A6).

REFERENCES

[1] D. Kaschiev, *Nucleation: Basic Theory with Applications* (Butterworth Heinemann, 2000).
[2] V. Carey, *Liquid Vapor Phase Change Phenomena: An Introduction to the Thermophysics of Vaporization and Condensation Processes in Heat Transfer Equipment*, 2nd ed. (Taylor & Francis, 2018), pp. 1–742.
[3] K. H. Chu, Y. Soo Joung, R. Enright, C. R. Buie, and E. N. Wang, Appl. Phys. Lett. **102**, 151602 (2013).
[4] A. R. Betz, J. Jenkins, C.-J. C. Kim, and D. Attinger, Int. J. Heat Mass Transfer **57**, 733 (2013).
[5] B. Bourdon, P. Di Marco, R. Rioboo, M. Marengo, and J. De Coninck, Int. Commun. Heat Mass Transfer **45**, 11 (2013).
[6] H. Kim, B. Truong, J. Buongiorno, and L. W. Hu, Appl. Phys. Lett. **98**, 083121 (2011).
[7] A. Prosperetti, Annu. Rev. Fluid Mech. **49**, 221 (2017).
[8] T. Kozynets, S. Fallows, and C. B. Krauss, Phys. Rev. D **100**, 052001 (2019).
[9] P. Reinke, Exp. Heat Transfer **10**, 133 (1997).
[10] A. D. Lavino, E. Smith, M. Magnini, and O. K. Matar, Langmuir **37**, 5731 (2021).
[11] M. Gallo, F. Magaletti, and C. M. Casciola, J. Fluid Mech. **906**, 20 (2021).
[12] G. Liang and I. Mudawar, Appl. Therm. Eng. **184**, 115982 (2021).
[13] Y. Chen, Y. Zou, B. Yu, D. Sun, and X. Chen, Nanoscale Microscale Thermophys. Eng. **22**, 198 (2018).
[14] B. Bourdon, R. Rioboo, M. Marengo, E. Gosselin, and J. De Coninck, Langmuir **28**, 1618 (2012).
[15] Y.-J. Chen, X.-J. Chen, B. Yu, Y. Zou, and W.-Q. Tao, Langmuir **36**, 13725 (2020).
[16] F. Caupin, J. Chem. Phys. **157**, 054506 (2022).
[17] S. G. Bankoff, AIChE J. **4**, 24 (1958).
[18] J. J. Lorenz, B. B. Mikic, and W. M. Rohsenow, *International Heat Transfer Conference Digital Library* (Massachusetts Institute of Technology Heat Transfer Laboratory, 1974), pp. 35–39.
[19] W. Tong, A. Bar-Cohen, T. W. Simon, and S. m. You, Int. J. Heat Mass Transfer **33**, 91 (1990).
[20] R. H. S. Winterton, J. Phys. D: Appl. Phys. **10**, 2041 (1977).
[21] C. H. Wang and V. K. Dhir, J. Heat Transfer **115**, 670 (1993).
[22] M. M. Mahmoud and T. G. Karayiannis, Therm. Sci. Eng. Prog. **25**, 101024 (2021).
[23] T. Yamamoto and M. Matsumoto, J. Therm. Sci. Technol. **7**, 334 (2012).
[24] B. R. Novak, E. J. Maginn, and M. J. McCready, J. Heat Transfer **130**, 042411 (2008).
[25] S. Acharya and B. Bagchi, J. Chem. Phys. **160**, 174503 (2024).
[26] S. Mukherjee, S. Datta, and A. K. Das, J. Heat Transfer **104**, 054503 (2018).
[27] Y. Liu, J. Tang, L. Li, Y. N. Shek, and D. Xu, Int. J. Heat Mass Transfer **132**, 25 (2019).
[28] X.-W. Lin, W.-T. Wu, Y.-B. Li, D.-W. Jing, B. Chen, and Z.-F. Zhou, Adv. Colloid Interface Sci. **334**, 103312 (2024).
[29] A. El-Rifai, S. Perumanath, M. K. Borg, and R. Pillai, J. Phys. Chem. C **128**, 8408 (2024).
[30] P. Rosales-Pelaez, M. I. Garcia-Cid, C. Valeriani, C. Vega, and E. Sanz, Phys. Rev. E **100**, 052609 (2019).
[31] C. P. Lamas, E. Sanz, C. Vega, and E. G. Noya, J. Chem. Phys. **158**, 124109 (2023).
[32] A. J. Page and R. P. Sear, Phys. Rev. Lett. **97**, 065701 (2006).
[33] S. Plimpton, J. Comput. Phys. **117**, 1 (1995).
[34] S. C. Maroo and J. N. Chung, J. Colloid Interface Sci. **328**, 134 (2008).
[35] Y. J. Chen, B. Yu, Y. Zou, B. N. Chen, and W. Q. Tao, Int. J. Heat Mass Transfer **158**, 119850 (2020).
[36] G. Nagayama and P. Cheng, Int. J. Heat Mass Transfer **47**, 501 (2004).
[37] X. D. Din and E. E. Michaelides, AIChE J. **44**, 35 (1998).
[38] J. L. Barrat and L. Bocquet, Phys. Rev. Lett. **82**, 4671 (1999).
[39] L. Zhang, J. Xu, G. Liu, and J. Lei, Int. J. Therm. Sci. **152**, 106325 (2020).
[40] P. Sullivan, D. Dockar, R. Enright, M. K. Borg, and R. Pillai, Int. J. Heat Mass Transfer **217**, 124657 (2023).
[41] M. P. Allen and D. J. Tildesley, *Computer Simulation of Liquids*, 2nd ed. (Oxford University Press, 2017) pp. 1–626.
[42] D. Dockar, M. K. Borg, and J. M. Reese, Langmuir **35**, 9325 (2019).
[43] P. Sullivan, D. Dockar, M. K. Borg, R. Enright, and R. Pillai, J. Fluid Mech. **948**, 55 (2022).
[44] S. Marchio, S. Meloni, A. Giacomello, C. Valeriani, and C. M. Casciola, J. Chem. Phys. **148**, 064706 (2018).
[45] S. Jiang and J. H. ter Horst, Cryst. Growth Des. **11**, 256 (2011).
[46] D. Turnbull, J. Chem. Phys. **20**, 411 (1952).
[47] M. Gallo and C. M. Casciola, Int. J. Multiphase Flow **179**, 104924 (2024).
[48] B. J. Garrison, T. E. Itina, and L. V. Zhigilei, Phys. Rev. E **68**, 041501 (2003).
[49] M. Gallo, F. Magaletti, A. Georgoulas, M. Marengo, J. D. Coninck, and C. M. Casciola, Nat. Commun. **14**, 6428 (2023).
[50] A. Giacomello, M. Chinappi, S. Meloni, and C. M. Casciola, Langmuir **29**, 14873 (2013).
[51] Q. Xiao, Y. Liu, Z. Guo, Z. Liu, D. Frenkel, J. Dobnikar, and X. Zhang, Eur. Phys. J. E **40**, 114 (2017).
[52] P.-G. de Gennes, F. Brochard-Wyart, and D. Quéré, *Capillarity and Wetting Phenomena* (Springer New York, 2004).
[53] J. Israelachvili, *Intermolecular and Surface Forces* (Academic Press, 2011).
[54] V. P. Carey and A. P. Wemhoff, J. Heat Transfer. **128**, 1276 (2006).

[55]J. Zhang, P. Wang, M. K. Borg, J. M. Reese, and D. Wen, Phys. Fluids **30**, 082003 (2018).
[56]K. H. Ardron and G. Giustini, Phys. Fluids **33**, 111302 (2021).
[57]A. Giacomello, J. Chem. Phys. **159**, 110902 (2023).
[58]Y.-J. Chen, Q. Cao, J. Li, B. Yu, and W.-Q. Tao, J. Mol. Liq. **311**, 113306 (2020).
[59]N. Di Pasquale and R. L. Davidchack, J. Chem. Phys. **153**, 154705 (2020).
[60]P. Rosales-Pelaez, I. Sanchez-Burgos, C. Valeriani, C. Vega, and E. Sanz, Phys. Rev. E **101**, 022611 (2020).
[61]R. C. Tolman, J. Chem. Phys. **17**, 333 (1949).
[62]H. Kanda, Wahyudiono, and M. Goto, Symmetry **13**, 1376 (2021).
[63]K. K. Tanaka, H. Tanaka, R. Angélil, and J. Diemand, Phys. Rev. E **92**, 022401 (2015).
[64]M. Blander, D. Hengstenberg, and J. L. Katz, J. Phys. Chem. **75**, 3613 (1971).
[65]P. Sullivan, D. Dockar, and R. Pillai (2025). "Nanoscale surface effects on heterogeneous vapour bubble nucleation," Durham University Collections. https://doi.org/10.15128/r1mc87pq34z